Journal of the Serbian Chemical Society
JSCS-info@shd.org.rs • www.shd.org.rs/JSCS
J. Serb. Chem. Soc. 80 (7) 877–888 (2015)
JSCS–4766
UDC 547.514.72+546.732:547.521+519.677:544.112–185
Original scientific paper

Nucleus-independent chemical shift profiles along the intrinsic distortion path for Jahn–Teller active molecules. Study on the cyclopentadienyl radical and cobaltocene

LJUBICA ANDJELKOVIĆ[1], MARKO PERIĆ[1#], MATIJA ZLATAR[1] and MAJA GRUDEN-PAVLOVIĆ[2*#]

[1]*Center for Chemistry, ICTM, University of Belgrade, Njegoševa 12, 11001 Belgrade, Serbia and* [2]*Faculty of Chemistry, University of Belgrade, Studentski Trg 12–16, 11001 Belgrade, Serbia*

(Received 7 November 2014, revised 11 March, accepted 12 March 2015)

Abstract: The aromatic/anti-aromatic behavior of the cyclopentadienyl anion (Cp^-), bis(η^5-cyclopentadienyl)iron(II) ($Fe(Cp)_2$), as well as of the Jahn–Teller (JT) active cyclopentadienyl radical ($Cp^\bullet$) and bis(η^5-cyclopentadienyl)-cobalt(II) ($Co(Cp)_2$) were investigated using density functional theory (DFT) calculations of the nuclear independent chemical shifts (*NICS*). According to the *NICS* values, pentagon ring in $Fe(Cp)_2$ is more aromatic than that of the isolated Cp^-. The *NICS* parameters were scanned along the Intrinsic Distortion Path (IDP) for $Cp^\bullet$ and $Co(Cp)_2$ showing anti-aromaticity, which decreased with increasing deviation from the high symmetry D_{5h} to the low symmetry (LS) C_{2v}. Changes in the *NICS* values along the IDP revealed that $Co(Cp)_2$ in the LS nuclear arrangement has aromatic character, in contrast to the case of $Cp^\bullet$.

Keywords: vibronic coupling; DFT; aromaticity; metallocene.

INTRODUCTION

Aromaticity, an intuitive concept in chemistry and physics, is considered as a property of systems that are thermodynamically stabilized due to cyclic electron delocalization. The delocalized electronic structure of aromatic compounds yields enhanced planarity, equalized bond lengths, enhanced stability due to the resonance, favoring substitution instead of addition that would be typical for isolated double bonds, and the ability to sustain ring currents when exposed to external magnetic fields. Contrary to the concept of aromaticity, the Jahn–Teller (JT) effect[1,2] induces unequalization of bond lengths, leading to the stabilization

* Corresponding author. E-mail: gmaja@chem.bg.ac.rs
# Serbian Chemical Society member.
doi: 10.2298/JSC141107025A

of a system upon distortion. The connection of aromaticity and the JT effect is of utmost importance, since both effects have been very useful in the characterization and interpretation of the structure, stability and reactivity of many molecules. For this reason, computational chemists seek the origin, explanation and understanding of these two phenomena. According to The Hückel molecular orbital (MO) theory,[3,4] species with $4n + 2$ π electrons are aromatic, whereas structures with $4n$ π electrons are defined as anti-aromatic. Structures with $4n+1$ π electrons with unpaired electrons in degenerate orbitals are JT active species, and are supposed to show anti-aromaticity.[5–8] Bearing in mind that the JT theorem states that a molecule with a degenerate ground electronic state distorts along non-totally symmetric vibrational coordinates, and in such a way removes the degeneracy and lowers the energy, the question naturally arises: How does the JT distortion influence the aromaticity/anti-aromaticity? Although it is well known that different criteria of aromaticity may lead to different overall conclusions,[9] nucleus-independent chemical shifts (*NICS*) provide a widely accepted quantitative measure of aromaticity/anti-aromaticity.[10,11] Furthermore, a scan of the *NICS* parameters along the intrinsic distortion path (IDP)[12–14] was found to be the method of choice in the analysis of the aromatic behavior of JT active species,[7,8,15] since the distortion path provides direct insight into the microscopic origin, mechanism and consequences of distortion.[13,14]

A detailed density functional theory (DFT) computational analysis was performed to investigate the aromaticity of the cyclopentadienyl anion (Cp^-), bis(η^5--cyclopentadienyl)iron(II) ($Fe(Cp)_2$), the cyclopentadienyl radical ($Cp^\bullet$) and bis(η^5-cyclopentadienyl)cobalt(II) ($Co(Cp)_2$). In spite of their relatively simple composition, the aromaticity of the JT active $Cp^\bullet$ and $Co(Cp)_2$ have not been fully rationalized so far. Therefore, the aim of this work was also to understand the influence of the JT effect on the aromatic behavior of these species. The *NICS* were determined for the reference non-JT active species, Cp^- and $Fe(Cp)_2$, and molecules prone to the JT effect, $Cp^\bullet$ and $Co(Cp)_2$. In order to preserve chemically important features, an analysis of the full *NICS* profile of $Cp^\bullet$ and $Co(Cp)_2$ along the IDP was performed.

METHODOLOGY

All the DFT calculations were realized using the Amsterdam Density Functional program package, ADF2013.01.[16-18] Geometry optimization of all the investigated molecules was performed using the local density approximation (LDA) characterized by the Vosko–Willk–Nusair (VWN) parametrization,[19] as well as using general gradient approximations (GGA), such as BP86,[20,21] PW91,[22] OPBE,[23] and S12g,[24] and hybrids B3LYP[25,26] and S12h.[24] All electron triple-zeta Slater-type orbitals (STO) plus one polarization function (TZP) basis set were used for all atoms. All calculations were spin-unrestricted. Analytical harmonic frequencies[27,28] were calculated in order to ascertain that the low symmetry (LS) structures correspond to the stationary points on the potential energy surfaces. Calculations of the *NICS* values were performed at the B3LYP/6-311+G* level of theory using the Gaussian 09W

program package using LDA optimized geometries.[21,29-31] The *NICS* parameters were calculated for ghost atoms located at the center of Cp^- and $Cp^\bullet$. In order to obtain the full profile of aromatic/anti-aromatic behavior, calculations of the *NICS* parameters were performed from 0 Å to 5 Å, in steps of 0.5 Å. In order to avoid the influence of the magnetic field of the central metal ion in metallocenes, the first *NICS* value was calculated 1 Å above the metal ion along the *z*-axis. For JT active species in a high symmetry (HS) nuclear arrangement, the *NICS* values were calculated imposing HS (D_{5h}) nuclear arrangement and LS (C_{2v}) of electron density. The *NICS* parameters for JT active species, $Cp^\bullet$ and $Co(Cp)_2$, were scanned along the IDP.

Intrinsic distortion path – IDP

The IDP method[12-14] is based on the fact that all the information about the vibronic coupling at the HS nuclear arrangement is also contained in the distorted LS minimum energy structure. Hence, the distortion is given as a superposition of all totally symmetric normal modes in the LS point group, linking the HS configuration with the LS structure. Every point on the potential energy surface can be represented by a 3*N* dimensional vector, *N* being the number of atoms, $\vec{R}_X$, using mass-weighted generalized coordinates relative to the origin. The geometry of the LS energy minimum obtained by DFT calculations was chosen to be the origin of the configuration space, $\vec{R}_{LS} = 0$. Within the harmonic approximation, it is possible to express $\vec{R}_X$ as a linear combination of N_{a1} totally symmetric normal coordinates in the LS:

$$\vec{R}_X = \sum_{k=1}^{N_{a1}} \omega_{Xk} \vec{Q}_k \tag{1}$$

where ω_{Xk} are weighting factors that represent the contribution of the displacements along the different totally symmetric normal coordinates to $\vec{R}_X$; $\vec{Q}_k$ are mass-weighted totally symmetric normal coordinates, which are the eigenvectors of the Hessian, obtained from the DFT frequency calculations in the LS minimum energy conformation. The corresponding eigenvalues are λ_k.

Within this model, the energy of any nuclear configuration $\vec{R}_X$, E_X, relative to the LS energy minimum, is expressed as the sum of the energy contributions of all the LS totally symmetric normal modes:

$$E_X = \sum_{k=1}^{N_{a1}} E_k = \frac{1}{2} \sum_{k=1}^{N_{a1}} \omega_{Xk}^2 \vec{Q}_k^2 \lambda_k \tag{2}$$

The force at any given point ($\vec{R}_X$), $\vec{F}_{Xk}$ is defined as a derivate of the energy over Cartesian coordinates and in the HS point, it indicates the main driving force for the JT distortion. The total force is represented as a vector sum of the individual forces:

$$\vec{F}_{X_{tot}} = \frac{1}{2} \sum_{k=1}^{N_{a1}} \omega_{Xk} \lambda_k M^{1/2} \vec{Q}_k = \sum_{k=1}^{N_{a1}} \vec{F}_{Xk} \tag{3}$$

where *M* is a diagonal $3N \times 3N$ matrix with atomic masses in triplicate as elements (m_1, m_1, m_1, m_2,…, m_n), and enables the calculation of the IDP exactly from the HS to the LS point. The above details about IDP can be found elsewhere.[12-14]

RESULTS AND DISCUSSION

The planar Cp^- in its singlet state with D_{5h} symmetry was optimized using several different levels of theory. All chosen exchange correlation (XC) functionals reproduced experimental geometrical parameters with sufficient accuracy,[32] Table I. The $Fe(Cp)_2$ molecule has two possible conformations, eclipsed D_{5h} and staggered D_{5d}. According to previous studies, the D_{5h} conformation is the global minimum on the potential energy surface.[33–38] The calculated bond lengths, Table I, are in excellent agreement with the experimental data,[39] and with earlier theoretical investigations.[40] Since all the functionals reproduced geometrical parameters with good accuracy, the *NICS* were computed at the B3LYP/ /6-311+G* level, using geometries obtained with the simplest LDA functional. Calculated *NICS* values for Cp^- and $Fe(Cp)_2$ are given in Table II. Previous sophisticated computational studies provide a rather satisfactory insight into the nature of the aromaticity of Cp^- and revealed that Cp^- is aromatic, which is in accordance with the herein presented results.[41–46] It is important to emphasize that the *NICS* parameters for Cp^- were computed at the center of the pentagon and at various distances from the center of the ring. In the case of $Fe(Cp)_2$, the starting point for the *NICS* calculation was 1 Å above the central metal ion following the *z*-axis. The *NICS* value calculated at 1.6 Å represent the *NICS* in the center of the pentagon ring of the cyclopentadienyl ligand. According to the results, both molecules show aromatic character, and $Fe(Cp)_2$ is more aromatic,

TABLE I. Selected bond lengths (Å) for the stationary points of the investigated molecules, calculated with different XC functionals

Molecule	Bond	LDA	BP86	PW91	OPBE	S12g	B3LYP	S12h	Exp.
Cp^- (D_{5h}, $^1A_1'$)	C–C	1.406	1.420	1.417	1.413	1.414	1.410	1.404	1.413[32]
$Fe(Cp)_2$ (D_{5h}, $^1A_1'$)	Fe–C	2.004	2.055	2.049	2.006	2.033	2.082	2.048	2.03[39]
	C–C	1.422	1.434	1.432	1.429	1.429	1.422	1.417	1.43[39]
$Cp\cdot$ (C_{2v}, $^2B_1$)	C–C	1.364	1.374	1.372	1.370	1.371	1.365	1.360	–
		1.424	1.439	1.436	1.432	1.432	1.432	1.426	
$Cp\cdot$ (C_{2v}, $^2A_2$)	C–C	1.455	1.471	1.468	1.462	1.463	1.465	1.457	–
		1.390	1.402	1.400	1.397	1.397	1.394	1.389	
$Co(Cp)_2$ (C_{2v}, $^2B_1$)	Co–C	2.029	2.091	2.084	2.038	2.070	2.129	2.092	2.119[50]
		2.070	2.134	2.128	2.080	2.112	2.175	2.137	
		2.098	2.155	2.149	2.108	2.135	2.185	2.151	
	C–C	1.434	1.447	1.445	1.441	1.441	1.435	1.429	1.429[50]
		1.415	1.426	1.424	1.421	1.421	1.415	1.409	
		1.402	1.412	1.410	1.408	1.408	1.400	1.396	
$Co(Cp)_2$ (C_{2v}, $^2A_2$)	Co–C	2.090	2.150	2.143	2.101	2.129	2.184	2.149	2.119[50]
		2.047	2.111	2.104	2.056	2.089	2.153	2.115	
		2.022	2.083	2.076	2.031	2.062	2.118	2.083	
	C–C	1.406	1.416	1.414	1.412	1.412	1.404	1.400	1.429[50]
		1.426	1.438	1.436	1.432	1.432	1.427	1.421	
		1.438	1.450	1.448	1.444	1.444	1.439	1.432	

Table II.[41–49] The isolated Cp^- ring has a *NICS* value of –12.52 ppm in the center, Table II. When two Cp^- rings are placed at the distance which they have in the $Fe(Cp)_2$ molecule (3.2 Å), the *NICS* parameter calculated at the center of one 5-membered ring was –12.13 ppm. Hence, the difference between the *NICS* parameters for the isolated Cp^- and for the Cp^- fragment in $Fe(Cp)_2$ is caused by the presence of the central metal ion.

TABLE II. Calculated *NICS* values (ppm) for Cp^- and $Fe(Cp)_2$ using LDA optimized geometries at various distances (Å) from the center of the molecules (for $Fe(Cp)_2$, the *NICS* calculated at 1.6 Å corresponds to the *NICS* value at the center of the Cp^- ligand)

Distance, Å	*NICS*	$NICS_{zz}$
	Cp^-	
0.0	–12.52	–15.95
1.0	–9.44	–33.70
2.0	–3.97	–17.86
3.0	–1.63	–7.87
4.0	–0.77	–3.87
5.0	–0.40	–2.13
	$Fe(Cp)_2$	
1.0	–103.47	–65.35
1.6	–42.14	–29.40
2.0	–31.15	–29.73
3.0	–9.46	–29.07
4.0	–2.44	–13.37
5.0	–0.95	–6.38

It is worth noting that $Cp^\bullet$ and $Co(Cp)_2$ have a hole and an unpaired electron, respectively, in a doubly degenerate highest occupied molecular orbital. Since it was previously shown that the eclipsed conformation is more stable and the JT effect does not depend on the rotation of the rings,[51] the discussion will be limited only to $Co(Cp)_2$ in the eclipsed conformation. The ground electronic state of the investigated species in D_{5h} symmetry is $^2E_1''$, which couples with the doubly degenerate vibration, e_2'. According to group theory considerations, the descent in symmetry goes from the D_{5h} to the C_{2v} point group, and thus, the state $^2E_1''$ splits into $^2A_2$ and $^2B_1$. The average bond distances for the distorted LS structures of $Cp^\bullet$ calculated at different levels of theory are consistent, Table I. The calculated bond lengths for $Co(Cp)_2$ are in accordance with experiments,[50] regardless of the choice of selected XC functional, Table I. Recently, the JT distortion in these molecules was analyzed in detail using a multideterminental DFT approach and the IDP method.[12,14,51–53] The calculated JT parameters of $Cp^\bullet$ and $Co(Cp)_2$ using a multideterminental DFT approach are given in Table III. The results for $Cp^\bullet$ obtained by Miller *et al.*, who used dispersed fluorescence spectroscopy, are considered to be the benchmark (E_{JT} = 1237 cm^{-1}).[54] The pre-

TABLE III. Results of the DFT calculations performed to analyze the JT effect in $Cp^{\bullet}$ and $Co(Cp)_2$; the energies are given in eV; the JT parameters E_{JT} and Δ are given in cm^{-1} and R_{JT} in $(amu)^{1/2}$Å

Molecule	Symmetry	LDA	BP86	PW91	OPBE	S12g	B3LYP	S12h
$Cp^{\bullet}$	D_{5h}, $^2E_1''$	–64.674	–59.989	–61.008	–60.966	–61.624	–67.948	–72.863
	D_{5h}, $^2A_2$	–64.653	–60.031	–61.042	–61.018	–61.658	–68.369	–73.402
	D_{5h}, $^2B_1$	–64.653	–60.031	–61.042	–61.018	–61.658	–68.369	–73.402
	C_{2v}, $^2A_2$	–64.808	–60.192	–61.203	–61.179	–61.817	–68.578	–73.596
	C_{2v}, $^2B_1$	–64.808	–60.192	–61.205	–61.179	–61.817	–68.578	–73.596
	E_{JT}, $^2A_2$	1244.5	1301.8	1294.5	1300.2	1281.6	1685.7	1567.9
	E_{JT}, $^2B_1$	1244.5	1301.0	1312.3	1301.0	1284.0	1688.1	1568.8
	Δ	0.0	–0.8	–17.7	–1.6	–2.41	0.0	0.8
	R_{JT}, $^2A_2$	0.25	0.26	0.26	0.26	0.26	0.27	0.27
	R_{JT}, $^2B_1$	0.25	0.26	0.26	0.26	0.26	0.27	0.27
$Co(Cp)_2$	D_{5h}, $^2E_1''$	–142.290	–130.675	–133.049	–133.385	–134.525	–149.601	–161.584
	D_{5h}, $^2A_2$	–142.261	–130.690	–133.061	–133.381	–134.528	–150.140	–162.247
	D_{5h}, $^2B_1$	–142.261	–130.690	–133.061	–133.381	–134.528	–150.140	–162.246
	C_{2v}, $^2A_2$	–142.362	–130.785	–133.156	–133.485	–134.626	–150.230	–162.345
	C_{2v}, $^2B_1$	–142.362	–130.785	–133.156	–133.485	–134.626	–150.231	–162.344
	E_{JT}, $^2A_2$	813.8	762.2	761.4	838.0	783.9	727.5	791.2
	E_{JT}, $^2B_1$	813.8	761.4	759.8	839.6	785.6	729.1	785.6
	Δ	0.0	0.0	1.6	–1.6	0.0	–2.4	13.7
	R_{JT}, $^2A_2$	0.35	0.34	0.34	0.35	0.34	0.34	0.34
	R_{JT}, $^2B_1$	0.35	0.34	0.34	0.35	0.34	0.34	0.34

sent calculations at the LDA level gave a value of 1244 cm^{-1}, which is in great accordance with the experimentally obtained one, although all other XC functionals also give satisfactory results, Table III. The values of the JT stabilization energies in $Co(Cp)_2$, Table III, are in agreement with the value of 1050 cm^{-1} estimated from its solid state EPR spectra.[55] For both investigated JT active molecules, the warping barrier is close to zero, independent of the level of theory (Table III). The different ground states obtained by different XC functionals (Table III) are due to the very small warping barriers, which are within the range of the accuracy of the calculation. Furthermore, IDP analysis gave a deeper insight into the vibronic coupling in these JT active molecules.[14,53] In both molecules, it is possible to distinguish two distinct regions on the potential energy profile. In the first region, the energy changes faster, and most of the E_{JT} is achieved after 40 % of the path. In the second region, the change of the energy is small, the adiabatic potential energy surface is flat and the molecule just relaxes towards the global minimum. Three vibrations are most important for the distortion in Cp: C–C stretch, C–C–C bend, and C–C–H bend. These three modes were experimentally found to be the most significant.[54] In the case of $Co(Cp)_2$, the out-of-plane ring deformation and C–H wagging (the out-of-plane C–H bending), are the most important for the JT distortion. Although the JT effect in $Cp^{\bullet}$

and $Co(Cp)_2$ has often been studied,[54–56] the influence of the vibronic coupling on their aromatic character has not been investigated. The question is whether the distortion has a significant impact on the change of aromaticity. In $Cp^{\bullet}$ and $Co(Cp)_2$, the degeneracy of the $^2E_1''$ state is broken by the JT distortion that stabilizes the system. Therefore, the *NICS* parameters were computed at the LDA optimized geometries for both the HS and LS points on the potential energy surfaces. Observing the *NICS* values at the HS point of $Cp^{\bullet}$, a high anti-aromatic character is noticeable, Table IV. The calculated parameters for the global minimum of $Cp^{\bullet}$ show that it still possesses anti-aromatic character,[5] but much weaker than in the HS point, Table IV. Moving from the center of the pentagon ring along the *z*-axis, the *NICS* indices decrease. In the case of $Co(Cp)_2$, it is evident that molecule at the HS point has high anti-aromatic character, Table V. In the global minimum structure, $Co(Cp)_2$ shows σ aromaticity and π anti-aromaticity according to the *NICS* and $NICS_{zz}$ values, Tables IV and V.

TABLE IV. Calculated *NICS* values (ppm) for $Cp^{\bullet}$ using LDA optimized geometries at HS and LS geometries at various distances (Å) from the center of the ring; the *NICS* values for both LS structures are the same

Electronic state	Distance, Å	*NICS*	$NICS_{zz}$
	$Cp^{\bullet}$ (D_{5h})		
$^2B_1/^2A_2$	0.0	86.88	273.95
	1.0	72.10	217.30
	2.0	21.36	61.38
	3.0	6.65	18.12
	4.0	2.69	7.06
	5.0	1.34	3.40
	$Cp^{\bullet}$ (C_{2v})		
$^2B_1/^2A_2$	0.0	20.78	77.09
	1.0	14.79	45.84
	2.0	3.58	8.00
	3.0	0.91	0.87
	4.0	0.31	–0.12
	5.0	0.13	–0.22

Since dependence of the *NICS* parameters on the distortion, $\vec{R}_X$ / $\vec{R}_{JT}$, and distances (Å) from the center of the molecules gives a more detailed picture, the *NICS* parameters were monitored along the IDP path for $Cp^{\bullet}$ and $Co(Cp)_2$, Fig. 1 and 2, respectively. The *NICS* parameters were scanned only for the $^2B_1$ state, since those computed for the $^2A_2$ state were almost the same. Due to the non-totally symmetric electron density, both molecules in D_{5h} possess strong anti-aromatic character. Near the point of electron degeneracy, *i.e.*, near the HS nuclear arrangement, the HOMO–LUMO gap is substantially small, thus the *NICS* parameters have large positive values in the first region of the IDP (Figs. 1

TABLE V. Calculated *NICS* values (ppm) for $Co(Cp)_2$ using LDA optimized geometries at HS and LS geometries at various distances (Å) from central metal ion. The *NICS* value calculated at 1.7 Å corresponds to the *NICS* parameter in the center of the pentagon in $Co(Cp)_2$; The *NICS* values for both LS structures are the same

Electronic state	Distance, Å	*NICS*	$NICS_{zz}$
	$Co(Cp)_2$ (D_{5h})		
$^2B_1/^2A_2$	1.0	302.49	1135.98
	1.7	67.59	281.61
	2.0	42.20	182.76
	3.0	24.86	73.78
	4.0	9.80	24.48
	5.0	4.04	9.32
	$Co(Cp)_2$ (C_{2v})		
$^2B_1/^2A_2$	1.0	–3.91	209.45
	1.7	–10.86	42.41
	2.0	–11.11	21.41
	3.0	–1.64	–5.91
	4.0	–0.10	–5.08
	5.0	–0.04	–2.92

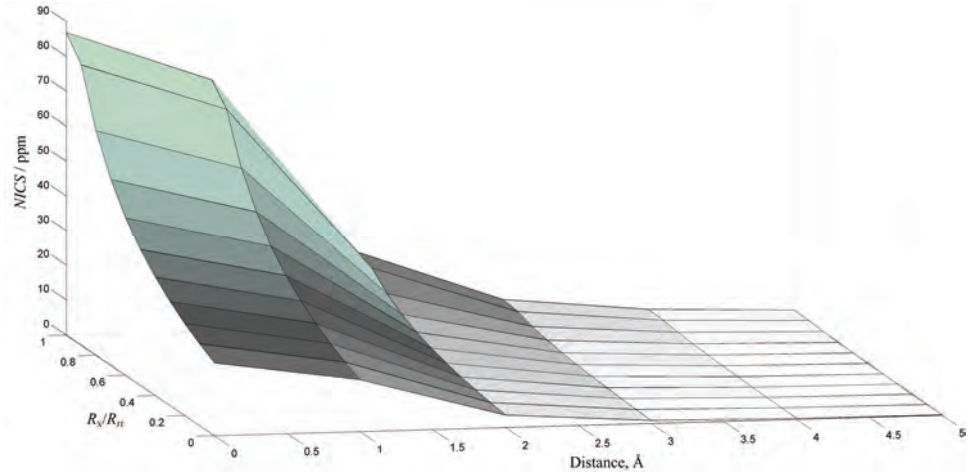

Fig. 1. Schematic plot of the *NICS* values along the IDP for $Cp^{\bullet}$ (from D_{5h} to C_{2v}), $^2B_1/^2A_2$ electronic states.

and 2). Going toward the global minimum point on the potential energy surface, the *NICS* values decrease and hence, the initially strong anti-aromatic character lowers, and finally, in the case of $Co(Cp)_2$, the *NICS* indices become negative, Figs. 1 and 2. It is worth noting that the negative *NICS* values in $Co(Cp)_2$ occur after 40 % of the IDP, where most of the JT stabilization is attained. The driving force responsible for the removal of orbital degeneracy leads to an enlargement of the HOMO–LUMO gap. Considering $Cp^{\bullet}$, for both the HS and LS nuclear arrange-

ment, the calculations revealed that the *NICS* decrease gradually along the *z*-axis, Fig. 1. Moving apart along the *z*-axis in the HS configuration of $Co(Cp)_2$, an abrupt decrease in the *NICS* parameters was observed until a distance of 1.7 Å (center of pentagon ring), Fig. 2. Going even further, the *NICS* parameters show a smooth decreasing trend, as expected.

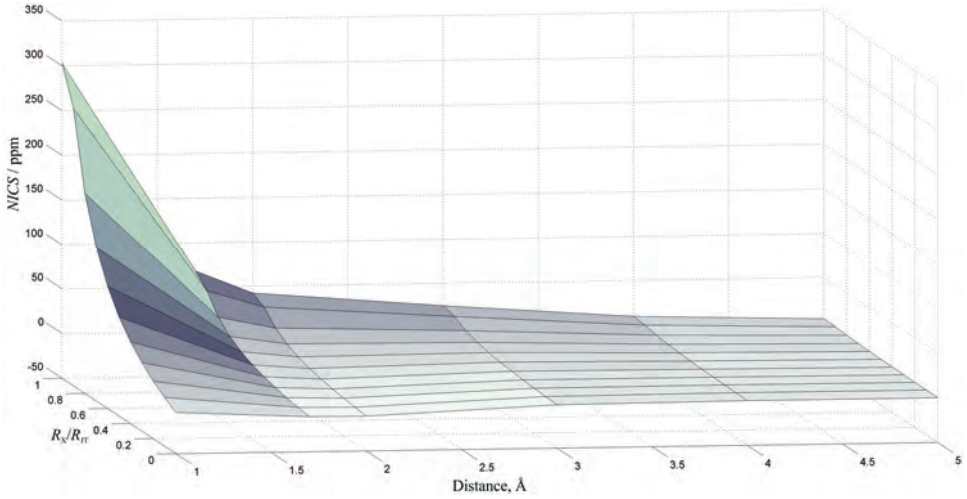

Fig. 2. Schematic plot of the *NICS* values along the IDP for $Co(Cp)_2$ (from D_{5h} to C_{2v}), $^2B_1/^2A_2$ electronic states.

CONCLUSIONS

Aromaticity is one of the oldest and most fundamental concepts in chemistry. The nature of aromatic compounds is very attractive, thus these species are among the most desirable synthetic targets. Since aromaticity is still awaiting comprehensive investigation, a detailed analysis of the *NICS* parameters, as one of the most widely used and efficient magnetic criteria, was performed in Cp^-, $Fe(Cp)_2$, $Cp^\bullet$ and $Co(Cp)_2$ by the means of DFT.

The calculations revealed that Cp^- and $Fe(Cp)_2$ are highly aromatic molecules. According to the *NICS*, the Cp^- ring in $Fe(Cp)_2$ is far more aromatic than the isolated Cp^-, showing the impact of the Fe^{2+}. In other words, these results would be highly attractive in applied sciences for the design of new advanced materials with desired properties, and the understanding of electronic structure, chemical bonding and properties in a moiety of aromatic species.

A thorough study of the influence of the JT effect on the aromaticity is presently of the utmost importance due to the increasing development of material chemistry, and substantial differences in aromatic/anti-aromatic behavior of JT active molecules. Thus, finding a method of choice to determine both chemically relevant phenomena is essential since they lead to the different reaction pathways

and the connection of aromaticity and vibronic coupling demands tremendous caution. For this purpose, the monitoring of the *NICS* along the IDP was performed. Similarly to the previous studies,[7,8,15] the anti-aromaticity decreases with increasing deviation from the high symmetry D_{5h} structures to the low symmetry C_{2v} global minimum structures, confirming that the JT distortion represents a mechanism for reducing anti-aromatic character. In the LS structure of $Co(Cp)_2$, the *NICS* become even negative, revealing aromatic character, in contrast to $Cp^{\bullet}$.

Acknowledgement. This work was financially supported by the Ministry of Education, Science and Technological Development of the Republic of Serbia (Grant No. 172035).

И З В О Д

ПРОФИЛ ХЕМИЈСКИХ ПОМЕРАЊА НЕЗАВИСНИХ ОД ЈЕЗГРА ДУЖ СВОЈСТВЕНОГ ПУТА ДИСТОРЗИЈЕ ЗА МОЛЕКУЛЕ ПОДЛОЖНЕ ЈАН–ТЕЛЕРОВОЈ ДИСТОРЗИЈИ. ПРОУЧАВАЊЕ ЦИКЛОПЕНТАДИЕНИЛ РАДИКАЛА И КОБАЛТОЦЕНА.

ЉУБИЦА АНЂЕЛКОВИЋ[1], МАРКО ПЕРИЋ[1], МАТИЈА ЗЛАТАР[1] и МАЈА ГРУДЕН-ПАВЛОВИЋ[2]

[1]Центар за хемију, ИХТМ, Универзитет у Београду, Његошева 12, 11001 Београд и [2]Хемијски факултет, Универзитет у Београду, Студентски трг 16, 11001 Београд

Ароматичност/антиароматичност циклопентадиенил анјона (Cp^-), бис(η^5-циклопентадиенил)гвожђа(II) ($Fe(Cp)_2$), као и, циклопентадиенил радикала ($Cp^{\bullet}$) и бис(η^5-циклопентадиенил)кобалта(II) ($Co(Cp)_2$), молекула подложних Јан–Телеровој дисторзији, испитивана је коришћењем теорије функционала густине (DFT) за израчунавање хемијских померања независних од језгра (*NICS*). На основу израчунатих хемијских померања, петочлани прстен у $Fe(Cp)_2$ је ароматичнији него изоловани Cp^-. *NICS* вредности, праћене дуж својственог пута дисторзије за $Cp^{\bullet}$ и $Co(Cp)_2$, указују на антиароматичност испитиваних врста, која се смањује са снижењем симетрије од D_{5h} до C_{2v}. Промене у *NICS* параметрима дуж пута дисторзије показују да $Co(Cp)_2$ у ниској симетрији поседује ароматични карактер, за разлику од $Cp^{\bullet}$.

(Примљено 7. новембра 2014, ревидирано 11. марта, прихваћено 12. марта 2015)

REFERENCES

1. H. A. Jahn, E. Teller, *Proc. R. Soc. London, Ser. A* **161** (1937) 220
2. I. B. Bersuker, *The Jahn–Teller Effect*, Cambridge University Press, New York, 2006
3. E. Hückel, *Z. Phys.* **70** (1931) 204
4. E. Hückel, *Z. Phys.* **78** (1932) 628
5. A. D. Allen, T. T. Tidwell, *Chem. Rev.* **101** (2001) 1333
6. A. C. Tsipis, *Phys. Chem. Chem. Phys.* **11** (2009) 8244
7. Lj. Andjelković, M. Perić, M. Zlatar, S. Grubišić, M. Gruden-Pavlović, *Tetrahedron Lett.* **53** (2012) 794
8. M. Perić, Lj. Andjelković, M. Zlatar, C. Daul, M. Gruden-Pavlović, *Polyhedron* **80** (2014) 69
9. Z. Chen, C. S. Wannere, C. Corminboeuf, R. Puchta, P. von Ragué Schleyer, *Chem. Rev.* **105** (2005) 3842
10. P. von Ragué Schleyer, C. Maerker, A. Dransfeld, H. Jiao, N. J. R. van Eikema Hommes, *J. Am. Chem. Soc.* **118** (1996) 6317

11. H. Jiao, P. von Ragué Schleyer, *Angew. Chem. Int. Ed. Eng.* **35** (1996) 2383
12. M. Zlatar, C.-W. Schläpfer, C. Daul, in *The Jahn–Teller-Effect Fundamentals and Implications for Physics and Chemistry*, H. Koeppel, D. R. Yarkoni, H. Barentzen, Eds., Springer Series in Chemical Physics, Vol. 97, Springer, Berlin Heidelberg, 2009, Ch. 1, p. 131
13. H. Ramanantoanina, M. Zlatar, P. García-Fernández, C. Daul, M. Gruden-Pavlović, *Phys. Chem. Chem. Phys.* **15** (2013) 1252
14. M. Gruden-Pavlović, P. García-Fernández, Lj. Andjelković, C. Daul, M. Zlatar, *J. Phys. Chem., A* **115** (2011) 10801
15. M. Perić, Lj. Andjelković, M. Zlatar, A. S. Nikolić, C. Daul, M. Gruden-Pavlović, *Monatsh. Chem.* **144** (2013) 817
16. ADF2013.01. SCM, *Theoretical Chemistry*, Vrije Universiteit, Amsterdam, http://www.scm.com, accessed in July, 2015
17. C. F. Guerra, J. G. Snijders, G. te Velde, E. J. Baerends, *Theor. Chem. Acc.* **99** (1998) 391
18. G. te Velde, F. M. Bickelhaupt, S. J. A. van Gisbergen, C. F. Guerra, E. J. Baerends, J. G. Snijders, T. Ziegler, *J. Comput. Chem.* **22** (2001) 931
19. S. Vosko, L. Wilk, M. Nusair, *Can. J. Phys.* **58** (1980) 1200
20. A. D. Becke, *Phys. Rev., B* **38** (1988) 3098
21. J. P. Perdew, *Phys. Rev., B* **33** (1986) 8822
22. J. P. Perdew, in *Electronic Structure of Solids '91*, P. Ziesche, H. Eschrig, Eds., Akademie Verlag, Berlin, 1991, p. 11
23. M. Swart, A. W. Ehlers, K. Lammertsma, *Mol. Phys.* **102** (2004) 2467
24. M. Swart, *Chem. Phys. Lett.* **580** (2013) 166
25. A. D. Becke, *J. Chem. Phys.* **98** (1993) 5648
26. C. Lee, W. Yang, R. G. Parr, *Phys. Rev., B* **37** (1988) 785
27. A. Bérces, R. M. Dickson, L. Fan, H. Jacobsen, D. Swerhone, T. Ziegler, *Comput. Phys. Commun.* **100** (1997) 247
28. H. Jacobsen, A. Bérces, D. Swerhone, T. Ziegler, *Comput. Phys. Commun.* **100** (1997) 263
29. *Gaussian 09*, Revision A.01, Gaussian, Inc., Wallingford, CT, 2009
30. A. D. Becke, *J. Chem. Phys.* **84** (1986) 4524
31. J. P. Perdew, W. Yue, *Phys. Rev.* **33** (1986) 8800
32. R. E. Dinnebier, U. Behrens, F. Olbrich, *Organometallics* **16** (1997) 3855
33. N. Mohammadi, A. Ganesan, C. T. Chantler, F. Wang, *J. Organomet. Chem.* **713** (2012) 51
34. H. Koch, P. Jørgensen, T. Helgaker, *J. Chem. Phys.* **104** (1996) 9528
35. U. Hohm, D. Goebel, S. Grimme, *Chem. Phys. Lett.* **272** (1997) 328
36. K. Pierloot, B. J. Persson, B. O. Roos, *J. Phys. Chem.* **99** (1995) 3465
37. A. Haaland, J. E. Nilsson, *Acta Chem. Scand.* **22** (1968) 2653
38. M. Swart, *Inorg. Chim. Acta* **360** (2007) 179
39. E. A. Seibold, L. E Sutton, *J. Chem. Phys.* **23** (1955) 1967
40. S. Coriani, A. Haaland, T. Helgaker, P. Jørgensen, *ChemPhysChem* **7** (2006) 245
41. J. Oscar, C. Jiménez-Halla, E. Matito, J. Robles, M. Sola, *J. Organomet. Chem.* **691** (2006) 4359
42. T. M. Krygowski, M. K. Cyrański, *Chem. Rev.* **101** (2001) 1385
43. V. I. Minkin, M. N. Glukhovtsev, B. A. Simkin, *Aromaticity and Antiaromaticity: Electronic and Structural Aspects*, Wiley, New York, 1994
44. V. Ya. Lee, A. Sekiguchi, *Angew. Chem., Int. Ed.* **46** (2007) 6596

45. H. Jiao, P. von Ragué Schleyer, Y. Mo, M. A. McAllister, T. T. Tidwell, *J. Am. Chem. Soc.* **119** (1997) 7075
46. L. Nyulászi, P. von Ragué Schleyer, *J. Am. Chem. Soc.* **121** (1999) 6872
47. M. Laskoski, W. Steffen, M. D. Smith, U. H. F. Bunz, *Chem. Commun.* (2001) 691
48. D. E. Bean, P. W. Fowler, M. J. Morris, *J. Organomet. Chem.* **696** (2011) 2093
49. T. N. Gribanova, R. M. Minyaev, V. I. Minkin, *Open Org. Chem. J.* **5** (2011) 62
50. M. Yu. Antipin, R. Boese, N. Augart, G. Schmid, *Struct. Chem.* **4** (1993) 91
51. M. Zlatar, C.-W. Schläpfer, E. P. Fowe, C. Daul, *Pure Appl. Chem.* **81** (2009) 1397
52. L. Andjelković, M. Gruden-Pavlović, C. Daul, M. Zlatar, *Int. J. Quantum Chem.* **113** (2013) 859
53. M. Zlatar, M. Gruden-Pavlović, C.-W. Schläpfer, C. Daul, *J. Mol. Struc. THEOCHEM* **954** (2010) 86
54. B. E. Applegate, J. Bezant, T. A. Miller, *J. Chem. Phys.* **114** (2001) 4869
55. J. H. Ammeter, L. Zoller, J. Bachmann, P. Baltzer, E. R. Bucher, E. Deiss, *Helv. Chim. Acta* 64 (1981) 1063
56. B. E. Applegate, T. A. Miller, *J. Chem. Phys.* **114** (2001) 4855.